Cellular and Molecular Life Sciences (2019) 76:4995–5009
https://doi.org/10.1007/s00018-019-03157-7

ORIGINAL ARTICLE

Protein interacting with Amyloid Precursor Protein tail-1 (PAT1) is involved in early endocytosis

Aysegul Dilsizoglu Senol[1] · Lidia Tagliafierro[1,2] · Lucie Gorisse-Hussonnois[1] · Florian Rebeillard[1] · Léa Huguet[1] · David Geny[1] · Vincent Contremoulins[3] · Fabian Corlier[4] · Marie-Claude Potier[4] · Stéphanie Chasseigneaux[1,5] · Michèle Darmon[1] · Bernadette Allinquant[1]

Received: 4 September 2018 / Revised: 16 May 2019 / Accepted: 20 May 2019 / Published online: 28 May 2019

Abstract

Protein interacting with Amyloid Precursor Protein (APP) tail 1 (PAT1) also called APPBP2 or Ara 67 has different targets such as APP or androgen receptor and is expressed in several tissues. PAT1 is known to be involved in the subcellular trafficking of its targets. We previously observed in primary neurons that PAT1 is poorly associated with APP at the cell surface. Here we show that PAT1 colocalizes with vesicles close to the cell surface labeled with Rab5, Rab4, EEA1 and Rabaptin-5 but not with Rab11 and Rab7. Moreover, PAT1 expression regulates the number of EEA1 and Rab5 vesicles, and endocytosis/recycling of the transferrin receptor. In addition, low levels of PAT1 decrease the size of transferrin-colocalized EEA1 vesicles with time following transferrin uptake. Finally, overexpression of the APP binding domain to PAT1 is sufficient to compromise endocytosis. Altogether, these data suggest that PAT1 is a new actor in transferrin early endocytosis. Whether this new function of PAT1 may have consequences in pathology remains to be determined.

Keywords PAT1 · Neuron · Endocytosis · Transferrin uptake · Caspase cleaved APP

Introduction

Protein interacting with Amyloid Precursor Protein (APP) tail 1 (PAT1) also called APP binding protein 2 (APPBP2) or Ara 67 binds to three known targets such as APP [1], androgen receptor [2], or the Herpes Simplex Virus Type I Us11 gene product [3]. PAT1 is expressed in several human tissues and cell lines [2]. Its expression is high in breast cancers and ovarian adenocarcinomas with poor prognosis [4], in neuroblastoma [5], and in desmoplasmic medulloblastoma cerebellar tumors [6]. PAT1 has several domains including four tetratricopeptide repeat (TPR) motifs sharing homology with kinesin light chains which could facilitate its binding to microtubules. It is a cytosolic protein able to associate with membranes, like many proteins involved in vesicular trafficking [1]. The role of PAT1 in subcellular trafficking has been described for the three known targets [2, 3, 7, 8]. Indeed, we previously showed in primary neurons that PAT1 slows down APP trafficking to the cell surface [9]. Involvement of PAT1 in APP trafficking was also observed in neuroblastoma cells [10]. PAT1/Ara67 was shown to act as a repressor of androgen receptor transactivation, promoting the localization of androgen receptor in the cytoplasm rather than in

Electronic supplementary material The online version of this article (https://doi.org/10.1007/s00018-019-03157-7) contains supplementary material, which is available to authorized users.

✉ Bernadette Allinquant
bernadette.allinquant@inserm.fr;
bernadette.allinquant@gmail.com

[1] Faculté de Médecine, UMR_S894 INSERM, Université Paris Descartes, Sorbonne Paris Cité, 102-108 rue de la Santé, 75014 Paris, France

[2] Department of Neurology, Duke University Medical Center, Durham, NC 27710, USA

[3] ImagoSeine, Institut Jacques Monod, UMR 7592, CNRS and Université Paris Diderot, Paris, France

[4] Institut du Cerveau et la Moelle épinière, ICM, INSERM U 1127, CNRS UMR 7225, Sorbonne Universités, UPMC Univ Paris 06 UMR S 1127, Paris, France

[5] INSERM U1144, Université Paris Descartes and Université Paris Diderot UMR-S 1144, 75006 Paris, France

the nucleus [2]. Binding of PAT1 to Us11 results in altered distribution of both partners which may be important for the intracellular movement of viral components [3]. Whether the interaction of PAT1 to its targets regulates only subcellular trafficking remains to be determined.

APP is a transmembrane protein that gives rise to the production of amyloid peptides (Aß), key molecules in Alzheimer's disease (AD), after its sequential cleavage by beta and gamma secretases [11, 12]. PAT1 binds to the juxtamembrane cytoplasmic domain of APP, a region involved in its basolateral sorting (BaSS) in epithelial cells [13]. The tyrosine residue (Tyr^{653}) of the APP interaction domain is a key amino-acid for PAT1 interaction and for BaSS [13], and may be a sequence important for endocytosis. However, the interaction between PAT1 and APP is not crucial to APP endocytosis and subsequent gamma secretase cleavage [14]. Whether PAT1 interaction with the androgen receptor and Us11 is involved in endocytosis remains to be shown. In neuronal cells overexpressing PAT1a (99% identical to PAT1) and APP or its homologs, amyloid precursor-like proteins 1 or 2 (APLP1 or 2), the localization and morphology of PAT1a-containing vesicles in distal neurites suggested that they were secretory or endocytic vesicles [10]. In primary neuronal cells we observed that the interaction of APP and PAT1 is poor at the cell surface contrary to what was observed within the cytoplasm, while PAT1 appeared to be present in vesicles close to the plasma membrane [9]. Based on these results, we postulated that PAT1 could be associated with the endocytic vesicles. We show here that indeed PAT1 is associated to early endosomes and that it regulates the internalization/recycling of the transferrin receptor.

Materials and methods

Antibodies

Anti-myc Tag, anti-NCAM and anti-actin antibodies were purchased from Millipore, Saint-Quentin en Yvelines, France. Early Endosomal Antigen-1 (EEA1) was from ThermoFischer, Villebon sur Yvette, France. Rabbit polyclonal anti-Rab5 was from Cell Signaling, Ozyme, Saint Quentin en Yvelines, France. Anti-Rab11 was from Invitrogen, anti-Rab4 was from Abcam, Cambridge, UK and anti-Rab7 was from Santa Cruz Biotechnology, Heidelberg, Germany. Alexa 546 tagged transferrin was from Molecular Probes, ThermoFisher. Anti-Rabaptin 5 was a gift of Dr Zerial, Germany. Monoclonal anti-transferrin receptor antibody against the extracellular C-terminal part of the receptor [15], was from Thermofisher. The supernatant of the hybridoma cell line mAb26 was used as the antibody against PAT1 and was a gift of Dr Sanjay W Pimplikar [1]. Donkey anti-rabbit or anti-mouse antibodies labeled with Alexa 488 or Alexa 546 were from Jackson Immuno Research, Interchim, Montluçon, France.

Animals

Pregnant Swiss mice were purchased from SARL Janvier-Labs, (Le Genest Saint Isle, France).

Ethics statement

All animal procedures followed the French and European Union regulations. The protocol of animal euthanasia was performed according to French government ethical laws in strict accordance with the recommendations of the European Economic Committee (63/2010) and was approved by the local ethics committee (Direction Départementale des Services Vétérinaires de Paris, Service de la Protection de Santé Animale et de la Protection de l'Environnement).

Cell culture

Primary cortical neurons were prepared from E16 Swiss mouse embryos, as previously described in define medium [16, 17]. Dissociated cells were plated on 15 µg/ml polyornithine coated glass coverslips at a density of 15×10^4 neurons/cm^2 for immunocytochemistry, transferrin uptake and transferrin receptor recycling. For western blotting, peptide retrieval and cell surface biotinylation experiments, cells were plated on plastic culture dishes coated with 1.5 µg/ml polyornithine. For some experiments at 15 days in vitro (DIV) the medium was neurobasal A supplemented with 2% B27, 0.2% GlutaMAX, 0.1% penicillin/streptomycine (Millipore, Saint Quentin en Yvelines, France).

Small interfering RNA duplexes

Small interfering RNA duplexes (siRNAs) used to down-regulate PAT1 levels were purchased from Dharmacon (Cambridge, United Kingdom) (ID numbers: J-059477-10 and J-059477-12) and used at the final concentration of 100 nM. GAPDH siRNAs, used as a negative control, were from ThermoFisher, (Ambion AM4624). siRNAs linked to penetratin (PolyPeptide Laboratories, Strasbourg, France) were internalized by 2 DIV primary cortical neurons (1×10^5 cells per well) as previously described [16]. Briefly, 0.03 nmol of siRNAs and 0.3 nmol of penetratin per 10^5 cells were mixed in the medium, incubated at room temperature for 30 min and then added to the conditioned medium to a final volume of 300 µl. After 4 h at 37 °C, 300 µl of medium was added to the cells and cells were incubated for 48 h and fixed with 4% paraformaldehyde (PFA).

Transfection of primary neurons

1.5 µg of pcDNA3.1/myc-His-PAT1 plasmid previously constructed [9] was transfected into cortical neurons (7 DIV) at a density of 3×10^5 cells/well via Lipofectamin 2000 Reagent (Invitrogen) according to the manufacturer's instructions. 20 h later, the cells were washed three times in PBS, fixed with 4% PFA and processed for immunocytochemistry.

Immunocytochemistry

After treatments described above, neurons were fixed with 4% PFA for 30 min and rinsed three times with PBS. Saturation of non-specific binding sites was performed with 5% bovine serum albumin (BSA) in PBS. Primary antibodies diluted in PBS and incubated at 37 °C for 1 h. Cells were then washed three times with PBS. Secondary antibodies were diluted in 5% BSA in PBS and applied for 1 h at 37 °C. After five washes in PBS, cells were mounted with Vectashield mounting medium (Vector Laboratories) and sealed.

Peptide internalization and retrieval

APP-PAT1 binding domain (Jcasp peptide) was chemically synthesized with penetratin peptide covalently linked to its N-terminal, at a purity of 95–98% (Neomps, Strasbourg, France). In retrieval experiments, the same peptide with biotinylated penetratin at its N-terminal was used. Both peptides (2.4 µM final) were added to the medium of cells after five DIV as previously described [18, 19].

For peptide retrieval, cells were processed as previously described [18, 19]. Briefly, neurons were incubated with biotinylated Jcasp peptide (J), for 3 h. After three washes in PBS, cells were lysed in 50 mM Tris pH 7.4, 150 mM NaCl, 1% Triton X100 and protease inhibitors cocktail (complete, Roche, Sigma-Aldrich, Saint-Quentin Fallavier, France). Lysed cells were homogenized and incubated on ice for 30 min. After centrifugation, supernatants were mixed with streptavidin beads for 2 h at 4 °C. The beads were recovered by centrifugation, washed and bound proteins were eluted in Laemmli buffer.

Transferrin uptake and recycling of transferrin receptors

5 DIV cortical primary neurons at the density of 1×10^5 cells per coverslip were washed three times with PBS and incubated with Hank's Balanced Salt Solution (HBSS) without transferrin. Plates were put on ice for 30 min. Then the medium was removed and replaced by HBSS added with Alexa 546 transferrin and the plates were put again on ice for 30 min. Cells were then washed three times with cold PBS and after adding HBSS they were put back at 37 °C for different time points (5, 10, 15, 20, 25, 30 min). At each time point, cells were washed two times with PBS and a third wash was performed with the addition of 0.5 M NaCl prior to the fixation with 4% PFA.

For transferrin receptor recycling, cells were washed and incubated on ice for 30 min with HBSS. The medium was then replaced by HBSS containing 10 µg of human holotransferrin (Sigma) and incubated on ice for additional 30 min. After three washings with cold PBS the medium was replaced with pre-warmed HBSS and cells were incubated for 5, 10, 15 and 20 min at 37 °C. Cells were then processed for immunocytochemistry of the transferrin receptor for each time point.

Cell surface biotinylation

Cells were plated in 60 mm diameter dishes at a density of 1.5×10^6 cells. Half of the dishes were treated for PAT1 siRNAs at 2DIV (see above). Then 66 h later, cells were put for 10 min on ice and were rinsed gently with cold PBS and HBSS. Then the medium was replaced by cold HBSS containing 20 µg/ml of human holotransferrin and incubated on ice for 30 min. The cells were then washed with cold PBS and warm HBSS was added before incubation at 37 °C for 5, 10, 15, 20 min. After incubation time the cells were rinsed with cold PBS and incubated at 4 °C with PBS added of sulfo-NHS-biotin reagent (Life Technologies, Courtaboeuf, France) at 4 °C for 30 min. A part of the cells were not incubated at 37 °C and sulfo-NHS-biotin reagent in PBS was added. This time will be T0. At the end of the incubation time, cells were rinsed with PBS/glycine twice and PBS before scrapping and counting. Cell lysis was performed in 50 mM Hepes pH 7.5, 150 mM NaCl, 5 mM EDTA, 1% Triton X100, protease inhibitors (complete EDTA-free, Roche Diagnostics, Mannheim, Germany) for 1 h at 4 °C. After centrifugation at 4 °C at 14,000*g* for 15 min, the supernatant was added to magnetic streptavidin Sepharose beads (Fisher Scientific, Illkirch, France) and incubated with agitation at 4 °C. Then beads were washed with the same buffer and with the buffer added to 0.5 M NaCl and in 10 mM Hepes pH 7.5 and protease inhibitors. The pellet was then resuspended in Laemmli buffer.

Western blotting

Standard SDS-PAGE was performed using 10% acrylamide gels. After electrophoresis, the proteins were transferred onto polyvinylidene difluoride (PVDF) membranes. Then the membranes were saturated in Tris buffered saline (TBS)-0.2% Tween containing 5% low fat milk, and incubated overnight at 4 °C with the primary antibodies. After three rinses with TBS-0.2% Tween, the membranes were incubated with species-specific peroxidase-conjugated secondary

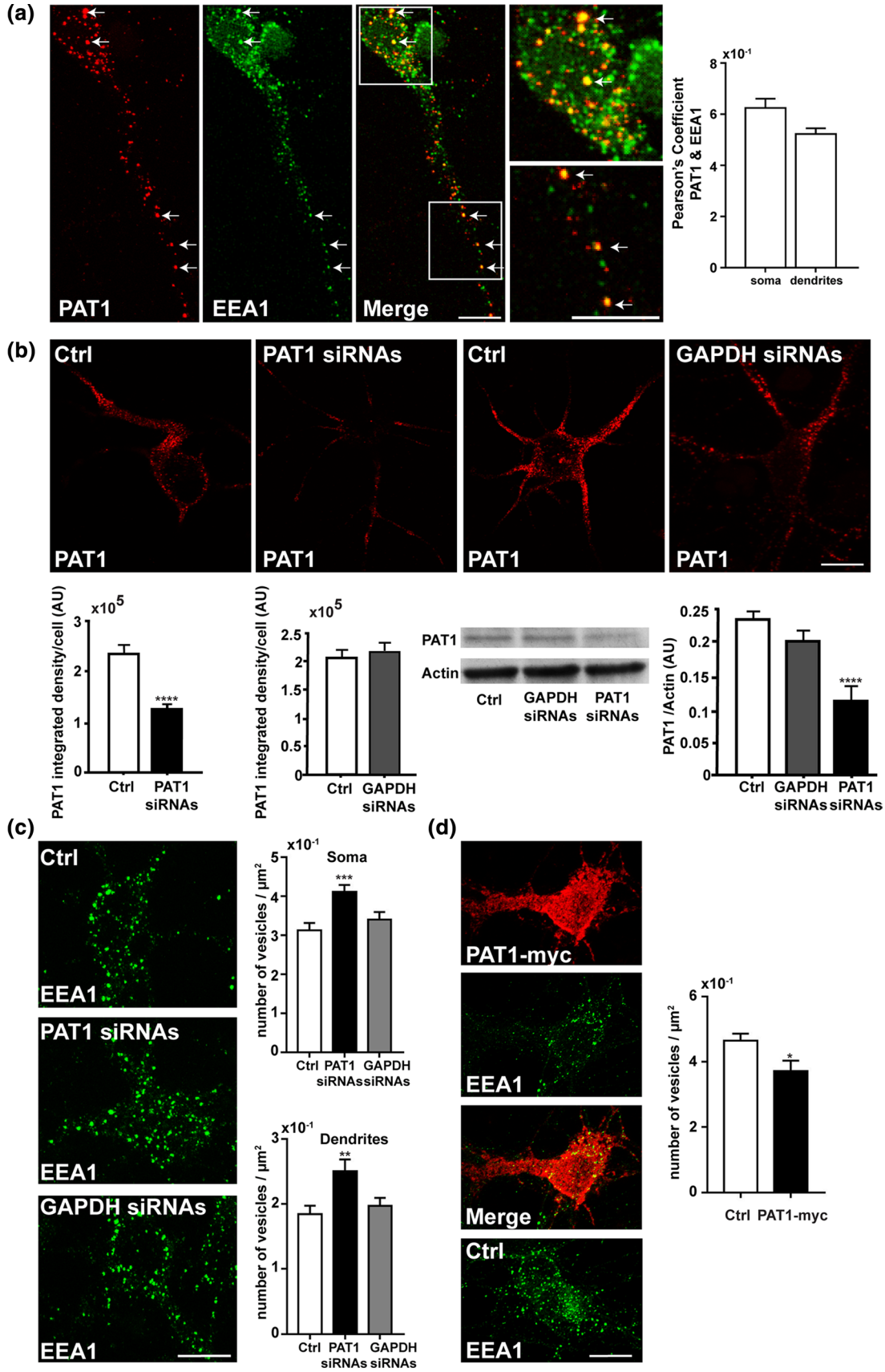
(a)
PAT1
EEA1
Merge
Pearson's Coefficient PAT1 & EEA1
x10-1
soma
dendrites
(b)
Ctrl
PAT1 siRNAs
PAT1
Ctrl
GAPDH siRNAs
PAT1
PAT1 integrated density/cell (AU)
x10^5
****
Ctrl
PAT1 siRNAs
PAT1 integrated density/cell (AU)
x10^5
Ctrl
GAPDH siRNAs
PAT1
Actin
Ctrl
GAPDH siRNAs
PAT1 siRNAs
PAT1 /Actin (AU)
****
Ctrl
GAPDH siRNAs
PAT1 siRNAs
(c)
Ctrl
EEA1
PAT1 siRNAs
EEA1
GAPDH siRNAs
EEA1
number of vesicles / µm2
x10-1
Soma
***
Ctrl
PAT1 siRNAs
GAPDH siRNAs
number of vesicles / µm2
x10-1
Dendrites
**
Ctrl
PAT1 siRNAs
GAPDH siRNAs
(d)
PAT1-myc
EEA1
Merge
Ctrl
EEA1
number of vesicles / µm2
x10-1
*
Ctrl
PAT1-myc

◂**Fig. 1** PAT1 colocalizes with EEA1 and regulates EEA1 vesicle number. **a** Neurons were fixed and immunolabeled for PAT1 (cy3) and EEA1 (Alexa 488). One representative immunolabeled confocal image and enlarged insets are presented. Colocalized vesicles are shown by arrows. Pearson's coefficient is shown (30 cells analyzed). **b** PAT1 siRNAs or GAPDH siRNAs were added to neurons at 2 DIV and incubated for 66 h before fixation and PAT1 immunocytodetection or extraction for western blots comparatively to control (Ctrl) in the absence of treatment. One representative confocal image for PAT1 immunolabeling of each siRNA condition is presented. Quantification was performed in image J and expressed as integrated density/cell in arbitrary unit (AU). Western blotting for PAT1 and actin was performed on 40 µg of cell extracts loaded. The ratio of PAT1/actin is expressed in arbitrary unit (AU). **c** Neurons treated by PAT1 siRNAs or GAPDH siRNAs for 66 h comparatively to control (Ctrl) in the absence of treatment were fixed and immunolabeled for EEA1. Endosomes labeled by EEA1 were analyzed by confocal microscopy. One representative EEA1 immunolabeling of each condition is shown. Quantification of the number of endosomes per cell surface (μm^2) in soma and dendrites is presented (30 cells per condition). **d** Overexpression of PAT1-myc was performed by the transfection of neurons at 7 DIV. Cells were incubated for 20 h prior to be fixed and immunolabeled for myc (cy3) and EEA1 (Alexa 488). Representative EEA1 immunolabelings of PAT1-myc expressor and of a non expressor as control (Ctrl) of the same experiment are shown. Quantification of endosome number per cell surface (μm^2) is presented (15 cells per condition). **a**–**d** Scale bar: 10 µm. Enlarged insets: 5 µm. $^{****}p < 0.0001$; $^{***}p < 0.001$; $^{**}p < 0.01$; $^{*}p < 0.05$

antibodies (Bio-Rad, Marnes-la Coquette, France) for 1 h at room temperature. The peroxidase signal was visualized using enhanced chemiluminescence (ECL, GE Healthcare). Quantification of immunoblots was performed using the Chemi-Doc Analyzer (Bio-Rad). Anti-PAT1 and anti-actin were always processed on the same membrane. For peptide retrieval experiments, the membranes were first processed for anti-PAT1 and then after stripping, for anti-Rab5.

Quantification of fluorescence intensity, number and size of the vesicles

Fluorescent images were acquired at the PICPEN platform (INSERM, UMR 894) using a TCS SP5 confocal imaging system equipped with diode pumped solid state 561 nm and HeNe 633 nm lasers (Leica Microsystems, Mannheim, Germany). Digital images were collected in a sequential mode using a 63× plan Apochromat oil immersion objective, with a numerical aperture of 1.4 and pinhole size "airy 1". For each experiment, laser intensity and image settings were adjusted and kept constant. Z stacks were performed with a step size of 0.5 µm.

When using Image J software, an algorithm of image processing was developed to quantify vesicle area and vesicle numbers for each cell. Cells were first manually isolated by drawing a region of interest (ROI) with the ImageJ freehand selection tool. The first step of the algorithm identified the pixels corresponding to vesicles. These pixels were obtained using filtering and mathematical morphology [20] in the following way; a median filter and a discrete Laplace operator were first applied to remove noise and to enhance the contrast inside of the cells. A fixed threshold combined with an exclusion of the smallest isolated areas was then used to obtain binary images. A watershed operation was finally applied to separate touching objects. The second step of the algorithm computed the number of separated objects and the area of each object.

Fluorescence density comparisons of PAT1 siRNAs comparatively to GAPDH siRNAs or to control in the absence of treatment were quantified by ImageJ. The ROI defining the contour of each cell was created by freehand selection tool and total integrated intensity was measured and presented as arbitrary units (AU). Same was performed for transferrin and EGF uptakes.

For co-localization analyses, ROI for each cell were created manually using ImageJ freehand selection tool. Co-localization was measured using JACoP Plugin using Costes' automatic threshold and presented as Pearson's coefficient.

For the 3D quantification of vesicle number and of their volume and fluorescence intensity Volocity software was used. First, a ROI was drawn to delimit each cell. An algorithm using different tools such as "find object" (clipped to the ROI) to detect the fluorescence intensity with defined thresholds for each labeled vesicle type, "exclude object by size" to eliminate too small objects and "separate touching objects" to segment vesicles close to each other were used. This algorithm allowed us to find the average vesicle volume and their number per ROI. For the quantification of size distribution of EEA1 positive vesicles having labeled transferrin, we first performed colocalization analysis using "calculate object colocalization" presented as Pearson's coefficient. Then, EEA1 positive vesicles colocalizing with labelled transferrin were further filtered by size ($< \text{or} > 1\ \mu m^3; > 1.5\ \mu m^3$). To assess the fluorescence intensities of total TfR and the TfR at the membrane an algorithm with Volocity's Find Object (clipped to the ROI) was used with defined thresholds. Data were expressed as volume of total TfR (μm^3)/volume of ROI (μm^3).

For all determinations, at least 15 cells of each condition for each experiment were examined.

Statistical analysis

Data are Mean ± SEM from at least three experiments. Statistical analyses were performed using either ANOVA followed by the post hoc Scheffe's or Bonferroni's tests, or Student's *t* test. Statistics and graph analyses were performed using StatView and GraphPad Prism Softwares.

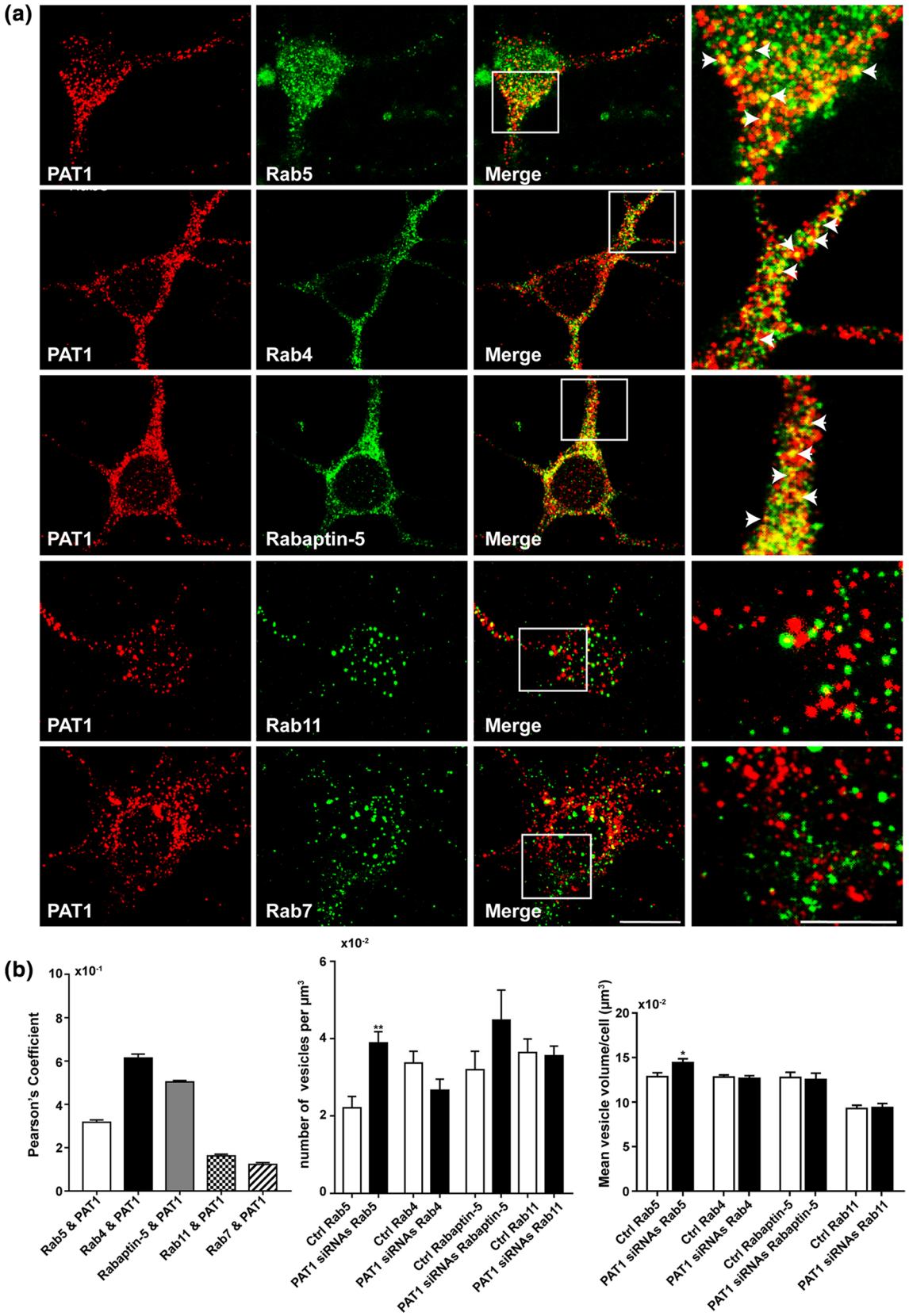
(a)
PAT1
Rab5
Merge
PAT1
Rab4
Merge
PAT1
Rabaptin-5
Merge
PAT1
Rab11
Merge
PAT1
Rab7
Merge
(b)
Pearson's Coefficient
x10-1
Rab5 & PAT1
Rab4 & PAT1
Rabaptin-5 & PAT1
Rab11 & PAT1
Rab7 & PAT1
number of vesicles per µm3
x10-2
**
Ctrl Rab5
PAT1 siRNAs Rab5
Ctrl Rab4
PAT1 siRNAs Rab4
Ctrl Rabaptin-5
PAT1 siRNAs Rabaptin-5
Ctrl Rab11
PAT1 siRNAs Rab11
Mean vesicle volume/cell (µm3)
x10-2
*

◂**Fig. 2** PAT1 colocalizes with Rab5, Rab4 and Rabaptin-5 and its down regulation increases Rab5 labeled vesicle number and size. **a** Neurons were fixed and immunolabeled for PAT1 (cy3) and Rab5, or Rab4, or Rabaptin-5, or Rab11, or Rab7 (all Alexa 488 labeled). Representative immunolabeled confocal images are presented. Enlarged insets are presented on the right side of each panel. Arrowheads indicate colocalized vesicles. Scale bar: 10 µm except for enlarged inserts: 5 µm. **b** Left side: Pearson's coefficients of double labelings of PAT1 with Rab5, Rab4, Rabaptin-5, Rab11, Rab7 and illustrated in a (30 cells analyzed). Middle and right sides: quantification of the number and size of immunolabeled vesicles for Rab5, Rab4, Rabaptin-5, Rab11, after PAT1 siRNAs treatment and in control (Ctrl) in the absence of treatment. Number of immunolabeled vesicles per cell volume (μm^3) and mean volume per cell are shown (30 cells per condition). *$p < 0.05$; **$p < 0.01$

Results

PAT1 colocalizes with EEA1 positive vesicles in primary neurons and its expression regulates the number of EEA1 positive vesicles

To check whether PAT1 could be associated to the endocytic pathway, we double labeled cortical primary neurons with anti-PAT1 and anti-EEA1 antibodies. EEA1 is a well-established marker of early endosomes [21–23]. We observed a colocalization of PAT1 and EEA1 both in the soma and in the dendrites with a respective Pearson's coefficient of 0.62 ± 0.03 for soma and of 0.52 ± 0.02 for dendrites (Fig. 1a) suggesting an important function in both compartments of differentiating neurons. In more mature neurons the Pearson's coefficient remains high for each compartment 0.67 ± 0.02 for soma and 0.49 ± 0.02 for dendrites suggesting that PAT1 may also be involved at all stages of neuronal development (Fig. 1Sa).

We then investigated if modulation of PAT1 levels could have consequences on EEA1 vesicle number. To this end, we used specific siRNAs to down regulate PAT1 level, as previously described [9]. PAT1 level was evaluated by immunocytochemical staining and immunoblots of cell extracts 66 h later the addition of PAT1 siRNAs (Fig. 1b). A significant decrease of PAT1 expression of about 50% was observed in the cells treated with PAT1 siRNAs, while GAPDH siRNAs did not change the level of PAT1 (Immunocytochemistry: Ctrl vs PAT1 siRNAs: $p < 0.0001$; Ctrl vs GAPDH siRNAs: NS); (Western blotting: Ctrl vs PAT1 siRNAs: $p < 0.0001$; Ctrl vs GAPDH siRNAs: NS; GAPDH siRNAs vs PAT1 siRNAs: $p = 0.003$) (Fig. 1b). We observed that under PAT1 siRNAs, there was a significant increase in the soma of about 24% of EEA1 vesicle number per cell surface (μm^2) (Ctrl vs PAT1 siRNAs: $p < 0.001$; Ctrl vs GAPDH siRNAs: NS; PAT1 siRNAs vs GAPDH siRNAs: $p = 0.01$). This increase was about 26% in dendrites under the same conditions (Ctrl vs PAT1 siRNAs: $p < 0.01$; Ctrl vs GAPDH siRNAs: NS; PAT1 siRNAs vs GAPDH siRNAs: $p = 0.02$) (Fig. 1c). In more mature neurons at 15DIV a significant increase of about 15% in the soma under PAT1 siRNAs was still observed (Ctrl vs PAT1 siRNAs: $p = 0.04$) while no significant differences were observed in dendrites (Ctrl vs PAT1 siRNAs: NS) (Fig. 1S). Conversely, overexpression of PAT1-myc produced a significant decrease of about 20% in the number of EEA1 vesicles per cell surface (non transfected cells vs transfected cells: $p = 0.02$) (Fig. 1d).

Down regulation of PAT1 increases the number of Rab5 positive vesicles but not of recycling Rab4 and Rab11 vesicles

We first checked whether PAT1 colocalizes with other Rab-labeled vesicles involved in the endocytic pathway [24, 25]. As EEA1 is an effector of Rab5 involved in early endocytosis we immunolabeled primary neurons with anti-PAT1 and anti-Rab5 and observed a colocalization with a Pearson's coefficient of 0.31 ± 0.01 (Fig. 2). More specifically this Pearson's coefficient was 0.29 ± 0.02 for soma and 0.25 ± 0.02 for dendrites. In more mature neurons, the colocalization between Rab5 and PAT1 was higher as the Pearson's coefficient was 0.68 ± 0.02 for soma and 0.43 ± 0.03 for dendrites meaning that the involvement in early endocytosis of PAT1 could be higher in both compartments at this stage (Fig. 1Sa). We then examined the colocalization of PAT1 with Rab4 involved in early endocytic recycling and observed a colocalization with a Pearson's coefficient of 0.61 ± 0.02 (Fig. 2). We further used antibodies against Rab11, Rab7 and found that colocalization of PAT1 with either Rab11 or Rab7 was poor as shown by respective Pearson's coefficient of 0.16 ± 0.01 and 0.12 ± 0.01 (Fig. 2). We also observed a colocalization of PAT1 with Rabaptin-5, a Rab5 effector (Pearson's coefficient of 0.50 ± 0.01) (Fig. 2). These data strongly suggest that PAT1 may be involved in early endocytic/recycling pathway but not in slow recycling or late endocytosis. To confirm whether PAT1 modulates the number of early endosomes, we then examined the number of Rab5-, Rab4-, Rabaptin-5-, and Rab11-positive vesicles after PAT1 downregulation following siRNAs treatment. We observed that decreasing PAT1 level promotes the number of Rab5 positive vesicles per cell volume (control vs PAT1 siRNAs: $p < 0.001$) and increases their volume (control vs PAT1 siRNAs: $p < 0.05$). In contrary, no effect was observed on Rab4, Rab11 and Rabaptin-5 labeled vesicles, suggesting an effect of PAT1 on early endocytosis rather than on recycling (Fig. 2b).

Down regulation of PAT1 increases endocytosis of the transferrin receptor

We next addressed the effect of PAT1 downregulation on transferrin endocytosis. ANOVAs showed a significant effect

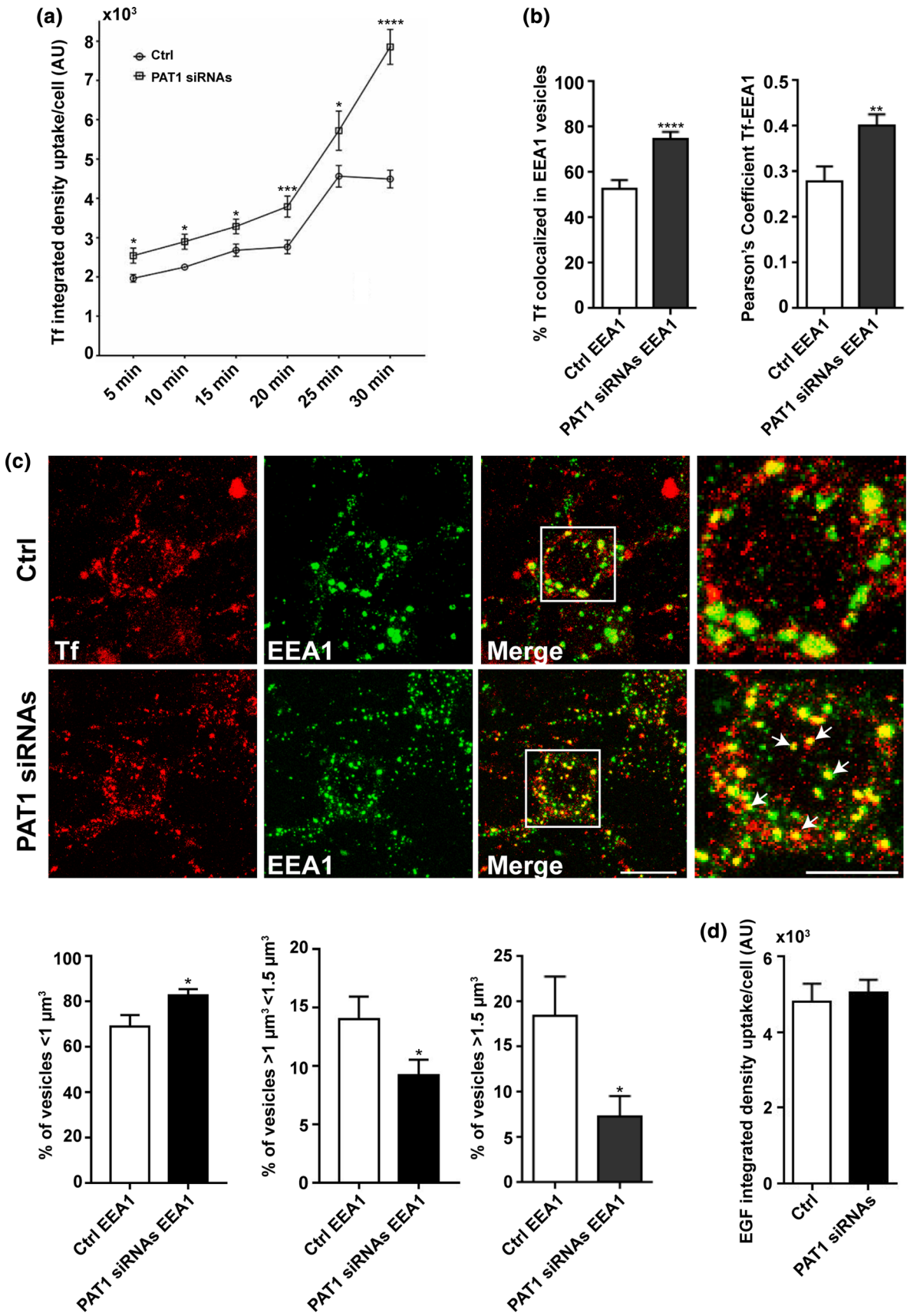
(a)
x10³
Tf integrated density uptake/cell (AU)
Ctrl
PAT1 siRNAs
5 min
10 min
15 min
20 min
25 min
30 min
(b)
% Tf colocalized in EEA1 vesicles
Ctrl EEA1
PAT1 siRNAs EEA1
Pearson's Coefficient Tf-EEA1
(c)
Ctrl
PAT1 siRNAs
Tf
EEA1
Merge
% of vesicles <1 µm³
% of vesicles >1 µm³<1.5 µm³
% of vesicles >1.5 µm³
(d)
EGF integrated density uptake/cell (AU)

◂**Fig. 3** Down regulation of PAT1 increases transferrin uptake in EEA1 vesicles. **a**–**c** Internalization of Alexa 546 tagged transferrin (Tf) was examined on neurons previously treated with PAT1 siRNAs and on control (Ctrl) in the absence of treatment. **a** Internalized Tf was evaluated and presented as integrated density/cell in arbitrary unit (AU). (25 neurons per condition). **b**, **c** Same experiment as in **a** in which the neurons were fixed and immunolabeled for EEA1, analyzed by confocal microscopy and quantified. **b** The % of Tf colocalized in EEA1 vesicles at 30 min and the Pearson's coefficient for EEA1-Tf are presented. (30 neurons per condition). **c** Representative image of internalized Alexa 546 tagged transferrin at 30 min and immunolabeled EEA1 vesicles is presented with enlarged insets on the right. Arrows indicated colocalized vesicles < 1 μm^3. Quantification of the vesicle volumes is presented and expressed in % of vesicles. (30 neurons per condition). Scale bar: 10 µm except for the enlarged insert: 5 µm. **d** Addition of Alexa 546 tagged EGF uptake was processed as for Alexa 546 transferrin. Quantification of internalized Alexa 546 EGF expressed by integrated density/cell in arbitrary unit (AU) is shown (30 neurons per condition). *$p < 0.05$; **$p < 0.01$; ***$p < 0.001$; ****$p < 0.0001$

of the treatment (PAT1 siRNAs versus control conditions: $F_{(1,48)} = 68.65$; $p < 0.0001$), of the time ($F_{(5,240)} = 69{,}82$; $p < 0.0001$) and of the interaction between treatment and time ($F_{(5,240)=}8{,}19$; $p < 0.0001$). In control conditions, we observed maximal transferrin internalization at 25 min which starts to decrease at 30 min (Fig. 3a). Down regulation of PAT1 induced a significant increase of internalized transferrin starting at early time points (ANOVA followed by Bonferroni's test: 5 min: control vs PAT1 siRNAs: $p = 0.016$; 10 min: control vs PAT1 siRNAs: $p = 0.02$; 15 min: control vs PAT1 siRNAs: $p = 0.03$; 20 min: control vs PAT1 siRNAs: $p = 0.002$; 25 min: control vs PAT1 siRNAs: $p = 0.047$; 30 min: control vs PAT1 siRNAs: $p < 0.0001$). The effects of PAT1 inhibition on internalized transferrin were highest at 30 min. This significant increase (about 40%) of internalized transferrin was also observed on more mature neurons (Fig. 1Sc). Altogether these results strongly suggest that low levels of PAT1 increase endocytosis which does not exclude some additional recycling defect as observed for the GTP-Rab5 Q79L dominant positive mutant [26].

We then wondered in which type of vesicles Alexa fluor 546 transferrin was accumulated. Same experiments were performed at all time points and neurons were immunolabeled after fixation using antibodies against EEA1, Rab5, Rab4, Rab11 and Rab7. At 30 min, the % of Alexa fluor 546-transferrin in EEA1 vesicles was the highest in control condition (52.94 ± 3.70) comparatively to Rab5 (7.86 ± 1.85), Rab4 (6.11 ± 1.28), Rab11 (6.71 ± 0.80), Rab7 (18.86 ± 6.18) labeled vesicles. We found that this % was significantly higher in PAT1 siRNAs conditions (74.66 ± 3.69; control vs PAT1 siRNAs: $p < 0.0001$), as was the Pearson's coefficient comparatively to the control conditions (control vs PAT1 siRNAs: $p = 0.005$) (Fig. 3b). No significant difference was observed in the mean volume of EEA1 vesicles between control and PAT1 siRNAs conditions in the absence of transferrin uptake (Fig. 2Sa). However, after 30 min of transferrin uptake, the % of colocalized vesicles (EEA1 and labeled transferrin) higher than 1.5 μm^3 or between 1.0 and 1.5 μm^3 were significantly lower in PAT1 siRNAs conditions (higher than 1.5 μm^3: control vs PAT1 siRNAs: $p = 0.037$; between 1.0 and 1.5 μm^3: control vs PAT1 siRNAs: $p = 0.04$) while the % of smaller vesicles less than 1 μm^3 was significantly higher under these conditions (control vs PAT1 siRNAs conditions: $p = 0.02$) (Fig. 3c). Indeed, at 5 min of Alexa fluor 546-transferrin uptake, transferrin did not colocalize with EEA1 vesicles. Colocalization was starting at 10 min and progressively increased with time until 30 min (Fig. 2Sb). However, at 10 and 20 min, the size of colocalized vesicles was not yet significantly different between control and PAT1 siRNAs conditions (Fig. 2Sc) except for vesicles of size between 1.0 and 1.5 μm^3 at 10 min (control vs PAT1 siRNAs conditions: $p = 0.03$) suggesting a delay in the fusion of vesicles at this time. These data suggest that low levels of PAT1 impede the fusion of endocytic vesicles with time comparatively to control conditions.

We did not observe any difference when repeating the same experiment using EGF between control and PAT1 siRNAs conditions thus suggesting that PAT1 low levels induce defects in static rather than in dynamic endocytosis [27, 28] (Fig. 3d).

We next checked transferrin endocytosis by measuring internalized transferrin receptor and analyzed its recycling at the cell surface. We first checked that PAT1 siRNAs did not induce any change in total and subcellular distribution of transferrin receptor (Fig. 4a). We observed a significant increase in total transferrin receptors in PAT1 siRNAs conditions at all time points (control vs PAT1 siRNAs: 5 min: $p < 0.0001$; 10 min: $p < 0.0001$; 15 min: $p < 0.001$; 20 min: $p < 0.0001$) (Fig. 4b). Similarly, membrane transferrin receptor was significantly increased as observed by immunocytodetection (control vs PAT1 siRNAs: 5 min $p < 0.001$; 10 min: $p < 0.0001$; 15 min: $p < 0.01$; 20 min: $p < 0.0001$) (Fig. 4b). In a new series of experiments we checked this increase in transferrin receptor at the membrane in PAT1 siRNAs conditions by cell surface biotinylation. We observed a significant increase in transferrin receptor with time which was significantly higher with PAT1 siRNAs at 5, 10, 15 min. At 20 min the differences between control and PAT1 siRNAs conditions were abolished (control vs PAT1 siRNAs: 5 min $p < 0.01$; 10 min: $p = 0.02$; 15 min: $p < 0.01$; 20 min: NS) (Fig. 4b). This could be explained by the fact that the % of transferrin receptor at the cell surface was significantly decreased with time starting from 10 min, as evaluated by immunocytochemical studies (control vs PAT1 siRNAs; 5 min: NS; 10 min: $p < 0.001$; 15 min: $p < 0.01$; 20 min: $p < 0.0001$) suggesting that neurons in which PAT1 expression was

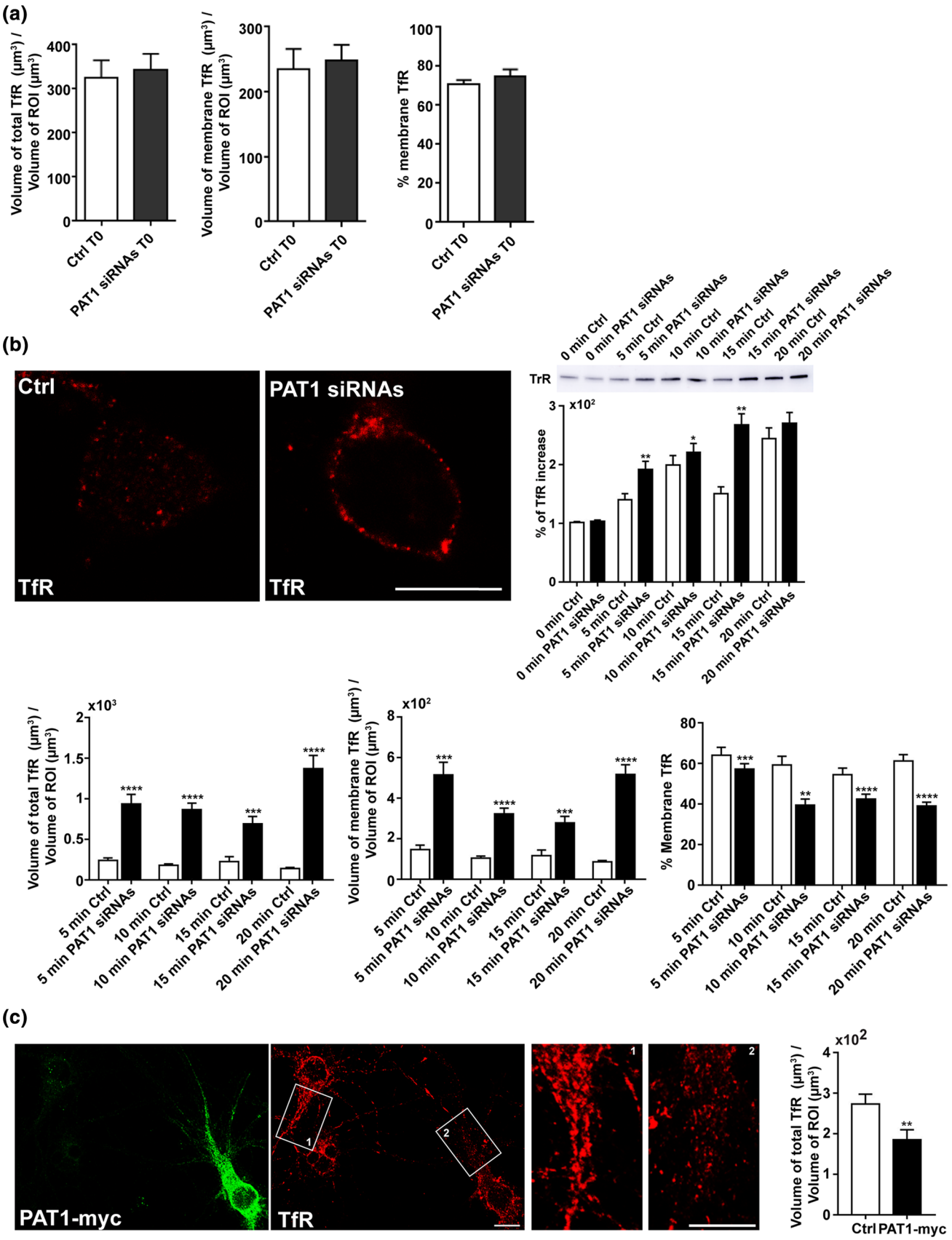
(a)
Volume of total TfR (µm³) / Volume of ROI (µm³)
Volume of membrane TfR (µm³) / Volume of ROI (µm³)
% membrane TfR
Ctrl T0
PAT1 siRNAs T0
(b)
Ctrl
TfR
PAT1 siRNAs
TfR
0 min Ctrl
0 min PAT1 siRNAs
5 min Ctrl
5 min PAT1 siRNAs
10 min Ctrl
10 min PAT1 siRNAs
15 min Ctrl
15 min PAT1 siRNAs
20 min Ctrl
20 min PAT1 siRNAs
TrR
% of TfR increase
x10²
Volume of total TfR (µm³) / Volume of ROI (µm³)
x10³
Volume of membrane TfR (µm³) / Volume of ROI (µm³)
% Membrane TfR
(c)
PAT1-myc
TfR
Volume of total TfR (µm³) / Volume of ROI (µm³)
Ctrl
PAT1-myc

◂**Fig. 4** Down and upregulation of PAT1 regulate Transferrin receptor. **a**, **b** Untagged transferrin was added to neurons previously treated with PAT1 siRNAs and to control (Ctrl) in the absence of treatment as described in Materials and Methods. At different time points cells were fixed (5, 10, 15, 20 min) and immunolabeled for transferrin receptor (TfR) and confocal analysis or proceeded for cell surface biotinylation. Total and membrane immunolabeled TfR were quantified and expressed as volume of total TfR (μm^3)/volume of ROI (μm^3) and of membrane TfR (μm^3)/volume of ROI (μm^3) respectively. The % of membrane TfR was reported to total TfR for each cell. For cell surface biotinylation, biotinylated membranes of $500x10^3$ cells were loaded. **a** Before incubation at different time points, some cells were proceeded for TfR immunolabeling and considered as T0. **b** Left: One representative confocal image of TfR at cell surface for control (Ctrl) and PAT1 siRNAs at 20 min and quantification for total, membrane immunolabeled TfR and % of membrane TfR are presented for each time point. Scale bar: 5 µm (30 cells for each condition). Right: One representative image of western blotting immunolabeled for TfR after cell surface biotinylation. Quantification was expressed by % of TfR increase at the different time points in control (Ctrl) or PAT1 siRNAs conditions comparatively to T0. **c** Overexpression of PAT1-myc was performed by the transfection of neurons at 7DIV and left for 20 h before fixation and immunolabeling of TfR (Alexa 546). One representative image of one PAT1-myc expressor in Alexa 488 and a non-expressor (Ctrl) in the same field is presented. Enlarged insets of TfR apical dendrite in Ctrl (1) and PAT1-myc expressor (2) are shown. Scale bar: 10 µm. Quantification was performed and expressed as volume of total TfR (μm^3)/volume of ROI (μm^3) (20 cells of each condition). *$p<0.05$; **$p<0.01$; ***$p<0.001$; ****$p<0.0001$

decreased, were not able to recycle the increased number of transferrin receptors internalized (Fig. 4b).

Conversely, overexpression of PAT1-myc lead to a significant decrease of about 35% of internalized transferrin receptor (Non transfected cells vs transfected cells: $p<0.01$) (Fig. 4c) confirming the involvement of PAT1 in endocytosis.

Increase in APP juxtamembrane cytoplasmic domain, significantly increases EEA1 vesicle number while reducing their size and decreases transferrin receptor internalization

PAT1 binds the 11 first amino-acids (KKKQYTSIHHG) of the APP juxtamembrane cytoplasmic domain [1], which is unmasked after APP caspase cleavage. We previously showed that overexpression in primary neurons of a peptide containing the PAT1 targeting domain extending to the caspase cleavage site, (Jcasp), induced translocation from the nucleus to the cytoplasm of the SET protein having several functions, as being an inhibitor of acetyl transferases, as a transcription factor, or an inhibitor of phosphatase 2A [16, 19, 29–31]. This mimicked what we observed in vivo in wild type mice overexpressing APP caspase cleaved [32]. To check if overexpression of Jcasp had consequences on endocytosis, we internalized the Jcasp domain peptide and examined the number of EEA1 vesicles per cell surface 3 h later at a time where the internalized peptide is not yet degraded [16]. We observed a significant increase in the number of EEA1 positive vesicles comparatively to control (control vs Jcasp: $p=0.03$) that had a smaller size (control vs Jcasp: $p<0.0001$) (Fig. 5a). Retrieval of the internalized peptide allowed to observe PAT1 bound to the peptide, as previously described, together with Rab5 (Fig. 5b). We then measured labeled transferrin internalization in cells overexpressing Jcasp. We observed a significant decrease of labeled internalized transferrin showing that endocytosis was compromised (control vs Jcasp: $p<0.01$) (Fig. 5c). These data suggest that overexpression of Jcasp domain mimicking the juxtamembrane cytoplasmic domain of APP caspase cleaved trapped PAT1 attached to other molecules, inducing a defect of transferrin endocytosis.

Discussion

We show here for the first time that PAT1, already known to be involved in trafficking of its targets [2, 3, 7–9] regulates early endocytosis, especially the transferrin receptor uptake/recycling and not the late endolysosomal pathway [33].

Vesicles of the endocytic pathway are characterized by regulatory cargos, all members of the Rab family of small GTPases localized to distinct membrane domains [24, 25]. Rab GTPAses are controlled by the recruitment of effector proteins. In this sense, Rabaptin-5 interacts with Rab5 thus stimulating its activity leading to an increase of transferrin uptake [34]. Rabaptin-5 interacts with Rab5 and Rab4 making a transition from the endocytic Rab5 to the rapid recycling Rab4 compartment [35]. Rabaptin-5 and Rab4 are necessary for regulating the formation of recycling vesicles [36]. Consequently and taken altogether our data suggest that PAT1 might modulate the action of Rabaptin-5 to Rab5 by stimulating its transition to Rab4 (Fig. 6a). This hypothesis would explain (1) high colocalization observed between PAT1 and Rab4 or PAT1 and Rab5 effectors i.e. Rabaptin-5 and EEA1, and between PAT1 and Rab5 under control conditions, (2) that low levels of PAT1 increase Rab5 vesicle number and size, increase EEA1 vesicle number and consequently increase transferrin uptake and transferrin receptor endocytosis and conversely, overexpression of PAT1 decreases EEA1 vesicle number and transferrin receptors internalized and (3) the decrease in the % of transferrin receptor recycling at the cell surface at low PAT1 levels which could probably be partly due to the very high level of transferrin receptors internalized. A decrease in recycling was also observed with the Rab5 mutant Q79L producing an increase of transferrin endocytosis [26]. This hypothesis requires further investigations.

PAT1 involvement in early endocytosis occurs both in young and mature neurons. In both cases, the higher

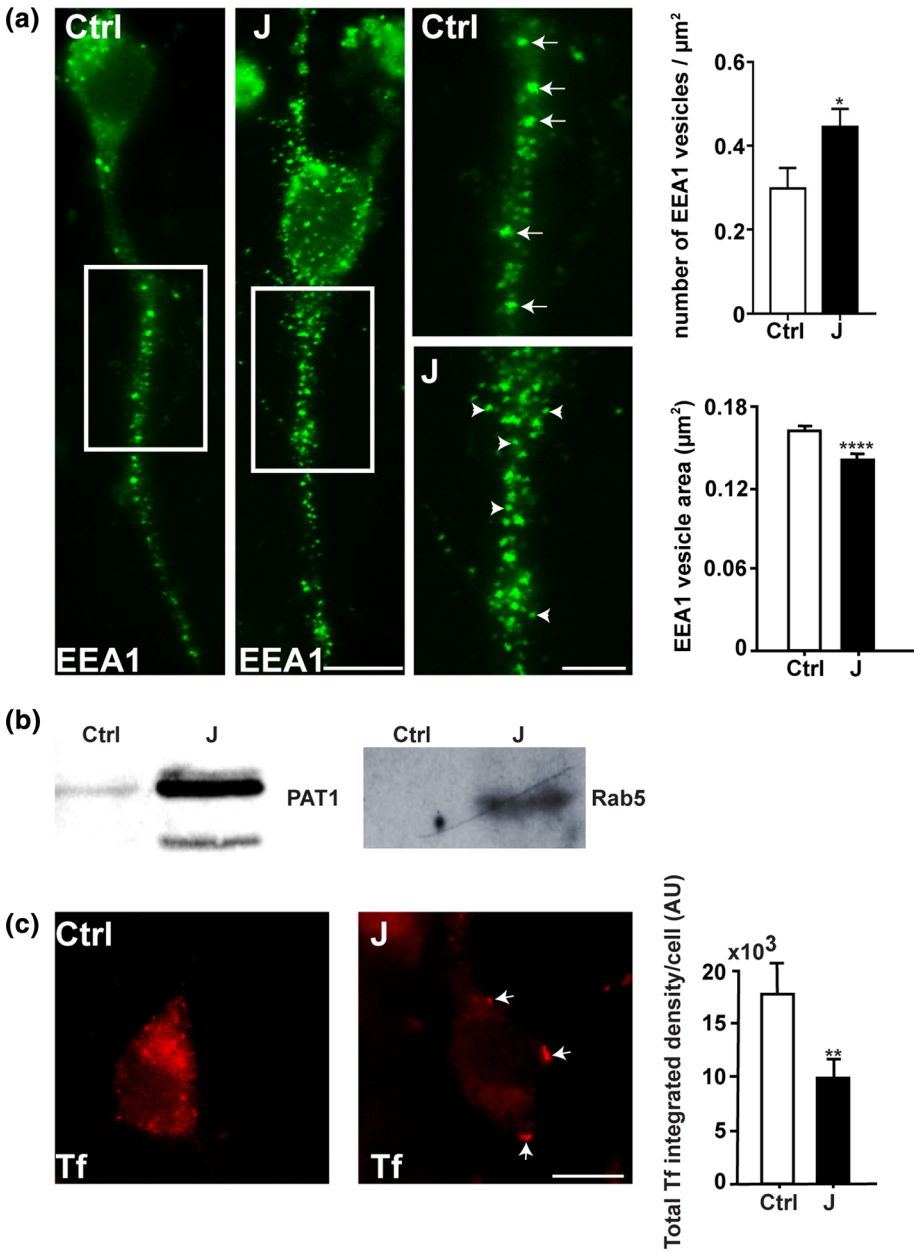

Fig. 5 Overexpression of the APP-PAT1 binding domain increases EEA1 labeled vesicles of smaller size and decreases transferrin uptake. **a** One representative image of immunolabeled EEA1 vesicles 3 h after internalization of APP-PAT1 binding domain peptide (J) comparatively to control (Ctrl) in the absence of treatment is shown. Enlarged insets are presented in the right side. Expression in number of vesicles per cell surface (μm^2) and vesicle area (μm^2) are shown (30 cells in each condition). Scale bar: 10 µm except for enlarged inset: 5 µm. **b** Peptide retrieval was proceeded as described in Materials and Methods on neurons having internalized biotinylated APP-PAT1 binding domain peptide (J) for 3 h. Proteins were analyzed by western blotting for PAT1 and Rab5. A control (Ctrl) in the absence of peptide was carried out in parallel. One representative immunoblot is presented. **c** Alexa 546 tagged transferrin (Tf) was added to primary neurons 3 h after the internalization of APP-PAT1 binding domain peptide (J) comparatively to control (Ctrl) in the absence of treatment. Internalized labeled transferrin 1 h later was analyzed by confocal microscopy (30 cells per condition). $^{**}p < 0.01$; $^{****}p < 0.0001$. Scale bar a, c: 10 µm

colocalization of PAT1 with EEA1 in the soma than in dendrites suggests that PAT1 acts mainly in the endocytosis of receptors in the soma. Whether endocytosis/recycling is higher in soma than in dendrites is not well documented and may vary with receptor types and their distribution [37, 38]. The higher colocalization of PAT1 with Rab5 in more mature than in young neurons may result from changes in the endocytic complex. We cannot exclude that additional partners may be more represented in more mature neurons leading higher PAT1 and Rab5 proximity, as compared to young neurons. Synaptic plasticity occurs in mature neurons where endocytosis/recycling plays an important role. We studied here the transferrin uptake through its receptor. Recent report shows that transferrin receptor controls the synaptic plasticity through the alpha-amino-3-hydroxy-5-methyl-4-isoxazolepropionic acid receptors [39]. Whether PAT1 levels may regulate synaptic plasticity remains to be determined. However, a similar transferrin uptake at low PAT1 levels was observed in young and more mature neurons in spite of the higher colocalization of PAT1 with Rab5 in more mature neurons than in young neurons. Additional physiological function of this high colocalization of PAT1 with Rab5 in more mature neurons remains to be determined. Rab5 controls the early endocytosis biogenesis [40]. In young neurons low levels of PAT1 have a stronger effect on the number of early endosomes than in mature neurons, suggesting that in mature neurons additional factors particularly in dendrites regulate the endosome number. The

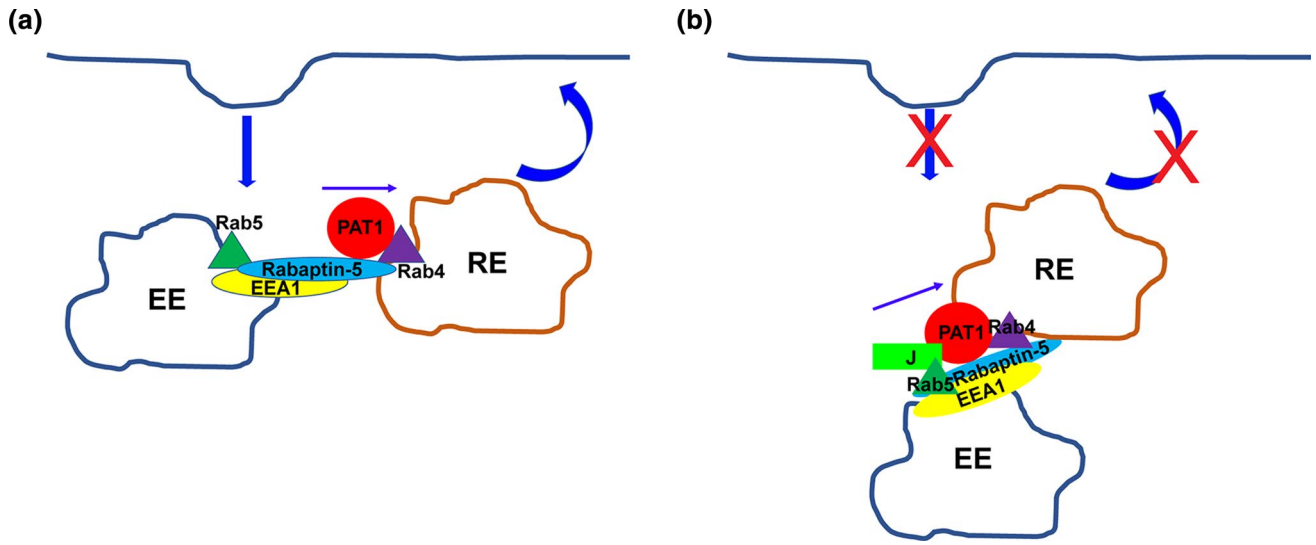

Fig. 6 Hypothetical model of the involvement of PAT1 in early endocytic pathway. **a** PAT1 interacts with Rab4 and the effectors of Rab5, Rabaptin-5 and EEA1 and might stimulate the transition from Rab5 to Rab4 from early endosomes (EE) to recycling endosomes (RE). **b** In presence of the J peptide PAT1 is trapped with its attached partners leading to their mislocalization and functional deficit of endocytosis and recycling

percentage of transferrin internalized in EEA1vesicles of size $> 1\ \mu m^3 < 1.5\ \mu m^3$ starts to decrease at low levels of PAT1 suggesting that PAT1 may be involved in the initiation of vesicles of higher size. This decrease in the percentage of large transferrin/EEA1 colocalized vesicles $> 1\ \mu m^3$ was still present 30 min after internalization when the transferrin uptake is maximal, in parallel to an increase with time in small vesicles lower than $1\ \mu m^3$. These data may suggest some defect in the fusion of vesicles at the origin of the formation of bigger vesicles compromising their recycling. This hypothesis requires further investigations.

PAT1 selectively binds to the first 11 amino-acids of the APP juxtamembrane cytoplasmic domain. However, when this APP sequence is extended to residue 29 or to the whole cytoplasmic domain, the binding with PAT1 is very low [1]. This could be due to the two type I reverse turns in the tertiary structure as the first type I turn at the TPEE 4 amino-acids downstream the caspase cleavage site may mask the APP/PAT1 domain of the APP cytoplasmic tail [41]. Increase of caspase cleavage in the cytoplasmic part of APP unmasked the interaction domain with PAT1. Such increase of APP caspase cleaved has been observed in the brain of AD patients and individuals with Down syndrome (DS) as well as in the hippocampus of Ts65Dn mice [42–45].

Endo-lysosomal pathway and particularly Rab5 is dysregulated in AD and in DS [46–49], and several mechanisms could be involved in these defects [50, 51]. PAT1 increases have also been observed with tumors of poor prognosis [4, 6]. Whether PAT1 may additionally interfere with the endocytic pathway in AD or DS or in the progression of tumors remains to be investigated.

Acknowledgements We thank Dr. Sanjay W. Pimplikar for mab26 to PAT1 and Dr. Marino Zerial for Rabaptin-5 antibody and Dr. Christophe Lamaze for helpful discussions. This work was supported by Institut National de la Santé et de la Recherche Médicale, France and by Fondation Jérôme Lejeune, France.

Compliance with ethical standards

Conflict of interest There are no actual or potential conflicts of interests between the authors and this work.

References

1. Zheng P, Eastman J, Vande Pol S, Pimplikar SW (1998) PAT1, a microtubule-interacting protein, recognizes the basolateral sorting signal of amyloid precursor protein. Proc Natl Acad Sci USA 95:14745–14750
2. Zhang Y, Yang Y, Yeh S, Chang C (2004) ARA67/PAT1 functions as a repressor to suppress androgen receptor transactivation. Mol Cell Biol 24:1044–1057
3. Benboudjema L, Mulvey M, Gao Y, Pimplikar SW, Mohr I (2003) Association of the herpes simplex virus type 1 Us11 gene product with the cellular kinesin light-chain-related protein PAT1 results in the redistribution of both polypeptides. J Virol 77:9192–9203
4. Hirasawa A, Saito-Ohara F, Inoue J, Aoki D, Susumu N, Yokoyama T, Nozawa S, Inazawa J, Imoto I (2003) Association of 17q21-q24 gain in ovarian clear cell adenocarcinomas with poor prognosis and identification of PPM1D and APPBP2 as likely amplification targets. Clin Cancer Res 9:1995–2004
5. Saito-Ohara F, Imoto I, Inoue J, Hosoi H, Nakagawara A, Sugimoto T, Inazawa J (2003) PPM1D is a potential target for 17q gain in neuroblastoma. Cancer Res 63:1876–1883
6. Ehrbrecht A, Muller U, Wolter M, Hoischen A, Koch A, Radlwimmer B, Actor B, Mincheva A, Pietsch T, Lichter P, Reifenberger G, Weber RG (2006) Comprehensive genomic analysis of

desmoplastic medulloblastomas: identification of novel amplified genes and separate evaluation of the different histological components. J Pathol 208:554–563
7. Gao Y, Pimplikar SW (2001) The gamma -secretase-cleaved C-terminal fragment of amyloid precursor protein mediates signaling to the nucleus. Proc Natl Acad Sci USA 98:14979–14984
8. Hsu CL, Chen YL, Ting HJ, Lin WJ, Yang Z, Zhang Y, Wang L, Wu CT, Chang HC, Yeh S, Pimplikar SW, Chang C (2005) Androgen Receptor (AR) NH2-and CooH-Terminal interactions result in the differential influences on the AR-mediated transactivation and cell growth. Mol Endocrinol 19:350–361
9. Dilsizoglu Senol A, Tagliaferro L, Huguet L, Gorisse-Hussonnois L, Chasseigneaux S, Allinquant B (2015) PAT1 inversely regulates the surface amyloid precursor protein level in mouse primary neurons. BMC Neurosci 16:10
10. Kuan YH, Gruebl T, Soba P, Eggert S, Nesic I, Back S, Kirsch J, Beyreuther K, Kins S (2006) PAT1a modulates intracellular transport and processing of amyloid precursor protein (APP), APLP1, and APLP2. J Biol Chem 281:40114–40123
11. Selkoe DJ (2001) Alzheimer's disease: genes, proteins, and therapy. Physiol Rev 81:741–766
12. Selkoe DJ, Wolfe MS (2007) Presenilin: running with scissors in the membrane. Cell 131:215–221
13. Haass C, Koo EH, Capell A, Teplow DB, Selkoe DJ (1995) Polarized sorting of beta-amyloid precursor protein and its proteolytic products in MDCK cells is regulated by two independent signals. J Cell Biol 128:537–547
14. Lai A, Sisodia SS, Trowbridge IS (1995) Characterization of sorting signals in the beta-amyloid precursor protein cytoplasmic domain. J Biol Chem 270:3565–3573
15. McClelland A, Kükn LC, Ruddle FH (1984) The human transferrin receptor gene: genomic organization, and the complete primary structure of the receptor deduced from a cDNA sequence. Cell 30:267–274
16. Briand S, Facchinetti P, Clamagirand C, Madeira A, Pommet JM, Pimplikar SW, Allinquant B (2011) PAT1 induces cell death signal and SET mislocalization into the cytoplasm by increasing APP/APLP2 at the cell surface. Neurobiol Aging 32:1099–1113
17. Chasseigneaux S, Dinc L, Rose C, Chabret C, Coulpier F, Topilko P, Mauger G, Allinquant B (2011) Secreted amyloid precursor protein beta and secreted amyloid precursor protein alpha induce axon outgrowth in vitro through Egr1 signaling pathway. PLoS One 6:e16301
18. Bertrand E, Brouillet E, Caillé I, Bouillot C, Cole GM, Prochiantz A, Allinquant B (2001) A short cytoplasmic domain of the amyloid precursor protein induces apoptosis in vitro and in vivo. Mol Cell Neurosci 18:503–511
19. Madeira A, Pommet JM, Prochiantz A, Allinquant B (2005) SET protein (TAF1beta, I2PP2A) is involved in neuronal apoptosis induced by an amyloid precursor protein cytoplasmic subdomain. Faseb J 19:1905–1907
20. Serra J (1982) Image analysis and mathematical morphology, vol 1. Academic Press, London, pp 1–610
21. Mu FT, Callaghan JM, Steele-Mortimer O, Stenmark H, Parton RG, Campbell PL, McCluskey J, Yeo JP, Tock EP, Toh BH (1995) EEA1, an early endosome-associated protein. EEA1 is a conserved alpha-helical peripheral membrane protein flanked by cysteine "fingers" and contains a calmodulin-binding IQ motif. J Biol Chem 270:13503–13511
22. Stenmark H, Aasland R, Toh BH, d'Arrigo A (1996) Endosomal localization of the autoantigen EEA1 is mediated by a zinc-binding FYVE finger. J Biol Chem 271:24048–24054
23. Simonsen A, Lippé R, Christoforidis S, Gaullier JM, Brech A, Callaghan J, Toh BH, Murphy C, Zerial M, Stenmark H (1998) EEA1 links PI(3)K function to Rab5 regulation of endosome fusion. Nature 394:494–498
24. Stenmark H (2009) Rab GTPases as coordinators of vesicle traffic. Nat Rev Mol Cell Biol 10:513–525
25. Vandinger-Ness A, Zerial M (2014) Rab proteins and the compartmentalization of the endosomal system. Cold Spring Harb Perspect Biol 6:a022616. https://doi.org/10.1101/cshperspect.a022616
26. Stenmark H, Parton RG, Steele-Mortimer O, Lutcke A, Gruenberg J, Zerial M (1994) Inhibition of rab5 GTPase activity stimulates membrane fusion in endocytosis. EMBO J 13:1287–1296
27. Lakadamyali M, Rust MJ, Zhuang X (2006) Ligands for clathrin-mediated endocytosis are differentially sorted into distinct populations of early endosomes. Cell 124:997–1009
28. Leonard D, Hayakawa A, Lawe D, Lambright D, Belive KD, Stanley C, Lifshitz LM, Fogarty KE, Corvera S (2008) Sorting of EGF and transferrin at the plasma membrane and by cargo-specific signaling to EEA1-enriched endosomes. J Cell Sci 121:3445–3458
29. Seo SB, McNamara P, Heo S, Turner A, Lane WS, Chakravarti D (2001) Regulation of histone acetylation and transcription by INHAT, a human cellular complex containing the set oncoprotein. Cell 104:119–130
30. Compagnone NA, Zhang P, Vigne JL, Mellon SH (2000) Novel role for the nuclear phosphoprotein SET in transcriptional activation of P450c17 and initiation of neurosteroidogenesis. Mol Endocrinol 14:875–888
31. Li M, Makkinje A, Damuni Z (1996) The myeloid leukemia-associated protein SET is a potent inhibitor of protein phosphatase 2A. J Biol Chem 271:11059–11062
32. Facchinetti P, Dorard E, Contremoulins V, Gaillard MC, Deglon N, Sazdovitch V, Guihenneuc-Jouyaux C, Brouillet E, Duyckaerts C, Allinquant B (2014) SET translocation is associated with increase in caspase cleaved amyloid precursor protein in CA1 of Alzheimer and Down syndrome patients. Neurobiol Aging 35:958–968
33. Mayle KM, Le AM, Kamei DT (2012) The intracellular trafficking pathway of transferrin. Biochem Biophys Acta 1820:264–281
34. Stenmark H, Vitale G, Ullrich O, Zerial M (1995) Rabaptin-5 is a direct effector of the small GTPase Rab5 in endocytic membrane fusion. Cell 83:423–432
35. Vitale G, Rybin V, Christoforidis S, Thornqvist P, McCaffrey M, Stenmark H, Zerial M (1998) Distinct Rab-binding domains mediate the interaction of Rabaptin-5 with GTP-bound Rab4 and Rab5. EMBO J 17:1941–1951
36. Pagano A, Crottet P, Prescianotto-Baschong C, Spies M (2004) In vitro formation of recycling vesicles from endosomes requires adaptor protein-1/clathrin and is regulated by rab4 and the connector rabaptin-5. Mol Biol Cell 15:4990–5000
37. Grady EF, Gamp PD, Jones E, Baluk P, McDonald DM, Payan DG, Bunnett NW (1996) Endocytosis and recycling of neurokinin 1 receptors in enteric neurons. Neuroscience 79:1239–1254
38. Shen A, Nieves-Citron M, Deng Y, Shi Q, Chowdhury D, Qi J, Hell JW, Navedo MF, Xiang YK (2018) Functionally distinct and selectively phosphorylated GPCR subpopulations co-exist in a single cell. Nat Commun 9:1050. https://doi.org/10.1038/s41467-018-03459-7
39. Liu K, Lei R, Li Q, Wang XX, Wu Q, An P, Zhang J, Zhu M, Xu Z, Hong Y, Wang F, Shen Y, Li H, Li H (2016) Transferrin receptor controls AMPA receptor trafficking efficiency and synaptic plasticity. Sci Rep 6:21019
40. Zeigerer A, Gilleron J, Bogorad RL, Marsico G, Nonaka H, Seifert S, Epstein-Barash H, Kuchimanchi S, Peng CG, Ruda VM, del Conte-Zerial P, Hengstler JG, Kalaidzikis Y, Koteliansky V, Zerial M (2012) Rab5 is necessary for the biogenesis of the endolysosomal system in vivo. Nature 485:465–470
41. Kroenke CD, Ziemnicka-Kotula D, Xu J, Kotula L, Palmer AG 3rd (1997) Solution conformations of a peptide containing the

cytoplasmic domain sequence of the beta amyloid precursor protein. Biochemistry 36:8145–8152
42. Ayala-Grosso C, Ng G, Roy S, Robertson GS (2002) Caspase-cleaved amyloid precursor protein in Alzheimer's disease. Brain Pathol 12:430–441
43. Banwait S, Galvan V, Zhang J, Gorostiza OF, Ataie M, Huang W, Crippen D, Koo EH, Bredesen DE (2008) C-terminal cleavage of the amyloid-beta protein precursor at Asp664: a switch associated with Alzheimer's disease. J Alzheimers Dis 13:1–16
44. Zhao M, Su J, Head E, Cotman CW (2003) Accumulation of caspase cleaved amyloid precursor protein represents an early neurodegenerative event in aging and in Alzheimer's disease. Neurobiol Dis 14:391–403
45. Dorard E, Gorisse-Hussonnois L, Guihenneuc-Jouyaux C, Albac C, Potier MC, Allinquant B (2016) Increases of SET level and translocation are correlated with tau hyperphosphorylation at ser202/thr205 in CA1 of Ts65Dn mice. Neurobiol Aging 46:43–48
46. Cataldo AM, Barnett JL, Pieroni C, Nixon RA (1997) Increased neuronal endocytosis and protease delivery to early endosomes in sporadic Alzheimer's disease: neuropathologic evidence for a mechanism of increased beta-amyloidogenesis. J Neurosci 17:6142–6151
47. Cataldo AM, Peterhoff CM, Troncoso JC, Gomez-Isla T, Hyman BT, Nixon RA (2000) Endocytic pathway abnormalities precede amyloid beta deposition in sporadic Alzheimer's disease and Down syndrome: differential effects of APOE genotype and presenilin mutations. Am J Pathol 157:277–286
48. Cataldo AM, Mathews PM, Boiteau AB, Hassinger LC, Peterhoff CM, Jiang Y, Mullaney K, Neve RL, Gruenberg J, Nixon RA (2008) Down syndrome fibroblast model of Alzheimer-related endosome pathology: accelerated endocytosis promotes late endocytic defects. Am J Pathol 173:370–384
49. Xu W, Fang F, Ding J, Wu C (2018) Dysregulation of Rab5-mediated endocytic pathways in Alzheimer's disease. Traffic 19:253–262
50. Cossec JC, Lavaur J, Berman DE, Rivals I, Hoischen A, Stora S, Ripoll C, Mircher C, Gratteau Y, OlivoMarin JC, de Chaumont F, Lecourtois M, Antonarakis SE, Veltman JA, Delabar JM, Duyckaerts C, di Paolo G, Potier MC (2012) Trisomy for synaptojanin1 in down syndrome is functionally linked to the enlargement of early endosomes. Hum Mol Genet 21:3156–3172
51. Kim S, Sato Y, Mohan PS, Peterhoff C, Pensalfini A, Rigoglioso A, Jiang Y, Nixon RA (2016) Evidence that the rab5 effector APPL1 mediates APP-ßCTF-induced dysfunction of endosomes in down syndrome and Alzheimer's disease. Mol Psychiatry 21:707–716